JACS
JOURNAL OF THE AMERICAN CHEMICAL SOCIETY

COMMUNICATION

pubs.acs.org/JACS

Zipping Up: Cooperativity Drives the Synthesis of Graphene Nanoribbons

Jonas Björk,[†] Sven Stafström,[*,†] and Felix Hanke[*,‡]

[†]Department of Physics, Chemistry and Biology, IFM, Linköping University, Sweden

[‡]Surface Science Research Centre, Department of Chemistry, University of Liverpool, Liverpool L69 3BX, U.K.

Supporting Information

ABSTRACT: We investigate the cooperative effects controlling the synthesis of a graphene nanoribbon on the Au(111) surface starting from an anthracene polymer using density functional calculations including van der Waals interactions. We focus on the high-temperature cyclodehydrogenation step of the reaction and find that the reaction proceeds by simultaneously transferring two H-atoms from the anthracene units to the Au surface, leaving behind a C−C bond in the process. This step is significantly more favorable than the three other potential reaction paths. Moreover, we find that successive dehydrogenations proceed from one end of the polyanthracene and propagate step-by-step through the polymer in a domino-like fashion.

This Communication describes a density functional theory study of the on-surface synthesis of graphene nanoribbons (GNRs) on Au(111), where we unravel the mechanisms that enable the growth of a GNR from a polymer precursor. The manufacturing of GNRs is of paramount interest for molecular-based electronics and in particular in field-effect transistor devices: in contrast to graphene,[1] they have a non-zero band gap, making them very interesting for semiconductor applications. The size of the band gap can be tuned by varying the width and shape of the edges[2] of the GNR. In order to tailor GNRs with desired properties, it is essential to first control their fabrication with predictable widths and shapes. Different approaches for creating GNRs have been suggested, such as edging,[3] lithography,[4] templated epitaxial growth,[5] and unzipping of carbon nanotubes.[6] Several recent studies[7−10] have been reported on the self-assembly of organic molecules into covalently coupled structures on various substrates, providing a successful route toward bottom-up GNR manufacturing with atomic precision.[7]

To understand covalent self-assembly, it is necessary to dissect the various interactions responsible for the on-surface reactions. Of particular interest is the catalytic role of the substrate on which the reactions take place. Theoretical literature exists, focusing for example on the cyclodehydrogenation of individual molecules[11] and the covalent coupling between molecules[12] on surfaces, but no in-depth computational studies on the self-assembly of GNRs have been reported to date. Theoretical insight is needed for a complete picture of the mechanisms responsible for the covalent self-assembly—and for mastering the control of different sizes and shapes.

Cai and co-workers recently reported[7] on the self-organization of the 10,10′-dibromo-9,9′-bianthryl molecule (DBBA) into GNRs on Au(111). The formation is enabled through a two-step process, depicted in Figure 1a. First the adsorbed monomers are dehalogenated, followed by covalent interlinking of the dehalogenated intermediates into polyanthracene. In the second step, the synthesis is finalized by cyclodehydrogenation of the polyanthracene into a well-defined GNR with a width of seven carbon atoms. The debromination step is becoming standard practice in today's chemistry toolkit and is reasonably well understood.[8,12] It is controlled by the dynamics of molecular diffusion on surfaces. The second step is associated with higher energetic barriers, which is reflected in the elevated activation temperature. Therefore, this is a crucial step to understand and is the focus of our current work. We illustrate the role and importance of the supporting Au(111) and underline the cooperative effects controlling the dehydrogenation process.

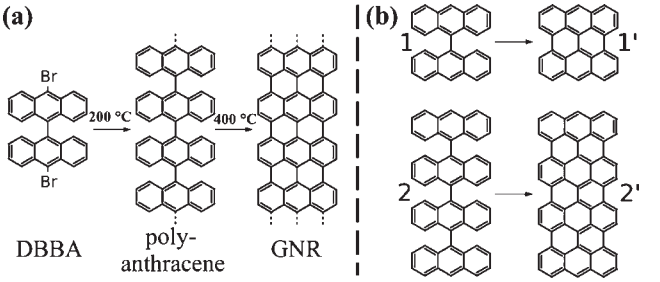

Figure 1. (a) Reaction scheme for the formation of linear graphene nanoribbons as reported by Cai and co-workers.[7] First, the precursor molecules dehalogenate and subsequently C−C couple to form linear polymers at a temperature of 200 °C. At a higher temperatures around 400 °C, these polymers undergo a cyclodehydrogenation, resulting in the graphene nanoribbon. (b) The two prototypical model systems used to investigate the cyclodehydrogenation in this study.

Our theoretical toolbox is based on periodic density functional theory (DFT) using the VASP code[13] interfaced to the Atomic Simulation Environment.[14] The van der Waals density functional[15] (vdW-DF) was used, as nonlocal correlations are required to describe the forces responsible for Au−C interactions,[16] while the PBE functional[17] was used to describe local correlation and semilocal exchange. This combination of exchange and correlation has proven successful for describing π-conjugated molecules on the Au(111) surface.[16] The latter has been represented in a supercell containing four Au layers separated by a 17 Å vacuum. The bottom two Au layers were kept fixed, while the remaining atoms were allowed to relax. The cyclodehydrogenation was studied for two prototypical model systems, illustrated in Figure 1b: a DBBA molecule with the Br-atoms replaced by H-atoms (bianthracene, **1**) and an oligo-anthracene consisting of four anthracene units

Received: June 23, 2011
Published: August 22, 2011

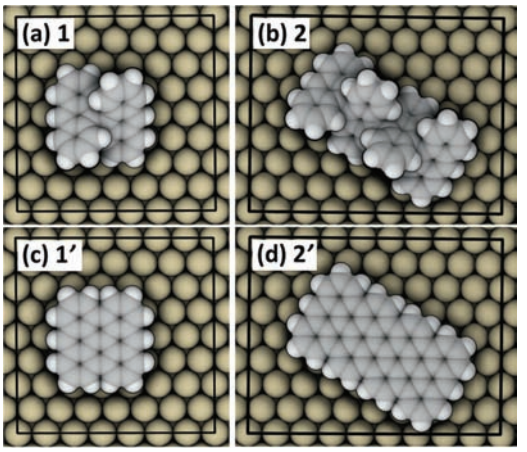

Figure 2. The most stable adsorption geometries of **1** and **2**, and their cyclodehydrogenated derivatives **1′** and **2′**, on the Au(111) surface. The surface unit cells used in the calculations are indicated with black lines.

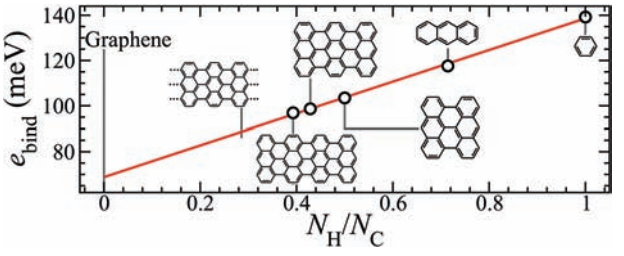

Figure 3. Binding energy normalized per number of C-atoms as a function of the hydrogen-to-carbon ratio for PAHs adsorbed on the Au(111) surface. Furthermore, extrapolated binding energies are indicated for the GNR under study and graphene on Au(111). Adsorption configurations are illustrated in Figure 2 for **1′** and **2′**, and in Figures S7−S9 for the other three PAHs.

(tetraanthracene, **2**). **1** and **2** cyclodehydrogenate into the polycyclic aromatic hydrocarbons (PAHs) **1′** and **2′**, respectively.

First, we model the adsorption of **1** and **2**, and their dehydrogenated derivatives **1′** and **2′**, on Au(111). The most stable adsorption configurations for the molecules are illustrated in Figure 2. The molecular orientation on the surface was found by comparing all high-symmetry adsorption sites for each molecule and choosing the one with the lowest energy, with no more than 5 meV per C-atom between orientations (see Supporting Information (SI)). The relevant binding energy, e_{bind}, is normalized by the number of C-atoms and predicts that **1** adsorbs slightly more strongly than **2** and is adsorbed closer to the surface than **2**. This behavior is assigned to steric hindrance, which is most dominant for **2**, with its two central anthracene units being rotated away from two adjacent anthracene units. The effect is smaller in **1**, where each anthracene unit has only one anthracene neighbor.

Compared to their precursors **1** and **2**, the two products **1′** and **2′** interact considerably more strongly with Au(111) since their flat geometry allows them to adsorb much closer to the surface. There is a significant difference in e_{bind} between **1′** and **2′**, although the two molecules adsorb at approximately 3.4 Å above the surface (see Table S1 in SI) . The difference in e_{bind} for **1′** and **2′** is in fact larger than that between the precursors **1** and **2**, which is assigned to the fact that **1′** has a higher hydrogen-to-carbon ratio than **2′**, making the former bind more strongly to the surface.

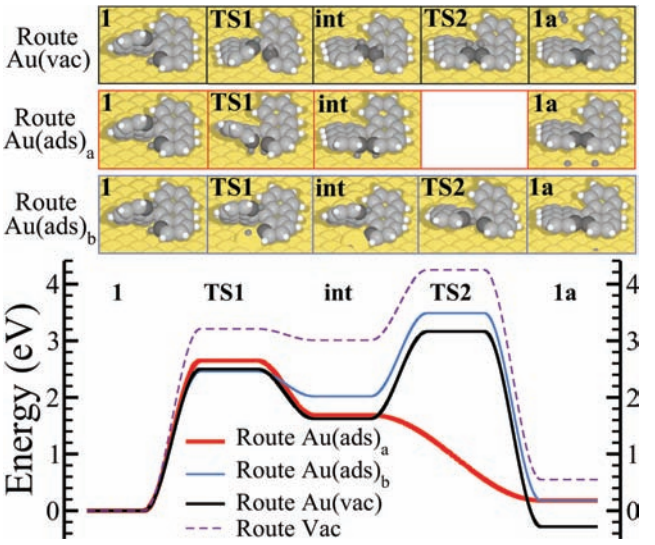

Figure 4. Energy diagram illustrating three reaction paths on Au(111) [routes Au(vac), Au(ads)$_a$, and Au(ads)$_b$] and one in vacuum [route Vac] for the cyclodehydrogenation of **1** into **1a**. The three reaction paths on the surface are depicted in the top of the figure as indicated by the legends and the color code. The states (structures) within the paths are labeled as denoted in the energy diagram plot. For routes Au(vac) and Vac, the dehydrogenated atoms are split off the molecule as molecular hydrogen, while for routes Au(ads)$_a$ and Au(ads)$_b$, they are adsorbed as atomic hydrogen to the surface. Note that for route Au(ads)$_b$, the H-atom adsorbed on the surface in **int** is assumed to diffuse across the surface and has therefore been removed in the calculations of the transition path from **int** to **TS2**.

The importance of the hydrogen atoms in the adsorbate is further illustrated in Figure 3, where e_{bind} is plotted as a function of the hydrogen-to-carbon ratio for **1′**, **2′**, and three additional PAHs. Note that the linear trend in the plot is merely a manifestation of the additivity of vdW interactions, for which a similar trend has been illustrated for PAHs adsorbed on graphene.[18] The linear trend in Figure 3 shows that the binding energy of any PAH adsorbed on the Au(111) surface can be described with

$$E_{bind} = N_C E_{CC} + N_H(E_{CH} - E_{CC}) \quad (1)$$

where N_C and N_H are the number of C-atoms and H-atoms of the PAH, respectively. E_{CC} (=70 meV) is the fitted adsorption energy per graphene-like carbon, and E_{CH} (=140 meV) is the fitted energy per benzene-like carbon and its adjoining H-atom; graphene-like carbons are C-atoms of the adsorbate featuring three covalent bonds with adjacent carbons, whereas benzene-like carbons are C-atoms covalently linked to two carbons and one hydrogen. Note that the trend in Figure 3 indicates that a benzene-like C-atom with its adjoining H-atom contributes almost twice as much to the adsorption of a PAH on Au(111) energy as a graphene-like C-atom. The result of this remarkable behavior is that the GNR will adsorb considerably more weakly than the two model systems. From eq 1, the extrapolated binding energy for an infinite GNR is 89 meV per C-atom, while we estimate 70 meV/atom for an extended graphene sheet adsorbed on Au(111).

To understand the formation of a GNR via the cyclodehydrogenation of polyanthracene, it is essential to investigate the catalytic effect of the gold surface. To this end, we computed a number of reaction pathways for a single dehydrogenation leading from **1** to **1a** (see Figure 4) both in vacuum and on Au(111), in which two H-atoms are split off and a new C−C bridge is formed. The net energy change for

each reaction step depends on the final state of the H-atoms. These can either be atomically adsorbed in an energetically favorable hollow site or react to form a gas-phase H_2 molecule. We chose the vacuum or on-surface hydrogen reference energies according to the final state in each reaction. The energy along the path is defined as

$$\Delta E = E_2 - E_1 + nE_H \quad (2)$$

where E_1 is the total energy of the initial system, and E_2 is the total energy of the corresponding transition, intermediate, or final reaction configuration. The integer n refers to the total number of H-atoms that have been split off to reach this particular state, and E_H is the reference energy for a single H-atom, which is taken either from its adsorbed form or from the gas phase as discussed above.

The *nudged elastic band* (NEB)[19] and *dimer*[20] methods were employed to identify the transition states (see SI). The energy barriers for the different paths are depicted in Figure 4. To avoid the high-energy product with atomic hydrogen in vacuum, the only plausible reaction path in vacuum results in a molecular hydrogen biproduct (route Vac). In this reaction two phenyl groups are rotated to first establish the new single C−C bond (state **int**), followed by the dissociation of molecular hydrogen, which leaves the final sp^2-type C═C bond. This reaction has previously been attempted in the gas phase and has not been seen at temperatures up to 1500 K.[21]

In the same reaction scheme on the surface (route Au(vac)), the configurations **TS1**, **TS2**, and **int** are lowered significantly in energy compared to their vacuum counterparts, showing the effect of flattening the bianthracene molecule upon adsorption. On Au(111), the energy barrier from **1** to **int** is found to be 2.50 eV, and for **int** to **1a** we obtain 1.54 eV. The inverse barrier from **int** to **1** is only 0.87 eV, which is considerably more favorable than completing the reaction. The low-energy barriers separating **int** from **1** in routes Vac and Au(vac) illustrate the low stability of the intermediates for these paths.

For the concerted route $Au(ads)_a$, in which the phenyl groups rotate toward the surface and the H-atoms adsorb on Au, only one transition barrier separates reactants from products. This barrier of 2.63 eV from **1** to **int** establishes a C−C bond and is 0.13 eV larger than the corresponding barrier for route Au(vac). However, within the numerical precision of the NEB method, no second energy barrier could be found that separates the configurations **int** and **1a**. The intermediate state **int** is either a saddle point or an extremely shallow minimum. In both cases, the dehydrogenation proceeds almost spontaneously once the initial transition state **TS1** has been found.

A third transition path on Au(111) was considered to explore the stepwise dehydrogenation and the potential formation of a metal−organic bond as an intermediate state. This is indicated as route $Au(ads)_b$ in Figure 4, for which two energy barriers were found. The first step splits off a H-atom from a C-atom and simultaneously pulls an Au-atom from the outmost layer of the substrate, forming a covalent bond. For the second barrier the remaining H-atom is transferred between the two C-atoms involved in the cyclodehydrogenation, followed by the spontaneous formation of a C−C bond and dehydrogenation. The energy barrier between the configurations **1** and **int** is 2.44 eV, and the one separating **int** from the final state **1a** is 1.47 eV. Note that the organometallic bond created between the molecule and one surface atom ensures that the molecule is not a radical in the intermediate state **int**.

From a comparison of the different reaction pathways presented in Figure 4, it is evident that the cooperative dehydrogenation route $Au(ads)_a$ is by far the most favored reaction path. Using Kramers's rate theory,[22] one can estimate that around 10^4 reactions proceed along route $Au(ads)_a$ for each reaction along route Au(vac) at the experimental temperature, while route $Au(ads)_b$ is still more unlikely. These results indicate that the majority of the H-atoms bind as atomic hydrogen to the Au(111) surface subsequent to the dehydrogenation. Thus, the gold surface has a true catalytic role for splitting of the H-atoms and does not only act as a support where the reaction can proceed.

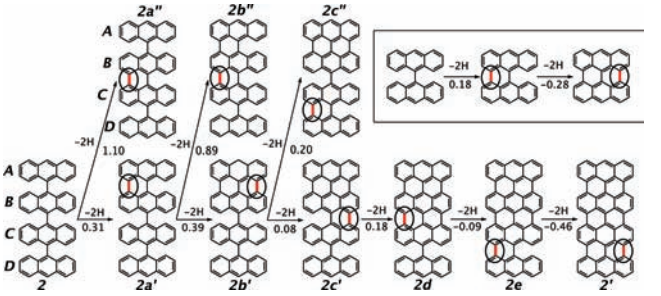

Figure 5. Reaction energies (in eV) for different reaction pathways of the cyclodehydrogenation **2** → **2′** (**1** → **1′** in the inset) on the Au(111) surface. The H-atoms that have been split off are assumed to bond to the Au(111) surface. Adsorption configurations of the intermediate structures are shown in Figure S6 (Figure S5 for **1** → **1′**).

The preference for the concerted pathway $Au(ads)_a$ is the reason why a noble gold surface is nearly ideal for the catalytic assembly of a GNR. The key is that Au(111) attracts the H-atoms sufficiently well to remove the second barrier but also has a high enough cohesive energy to make it too noble to provide Au adatoms[23] that could adversely affect the initial debromination step by forming C−metal−C bonds, which is seen for example on Cu surfaces.[9]

Having understood the catalytic role of the Au(111) surface, we now turn to investigate the order in which subsequent dehydrogenations proceed. The stepwise dehydrogenation for different reaction pathways of our two prototypical systems is illustrated in Figure 5. In each step, two H-atoms are split off and form an sp^2 bond between two C-atoms. At this stage, we consider only the energy differences between fully hydrogenated and fully dehydrogenated states, which are computed using eq 2. As reference energy for the H-atoms, we used atomic hydrogen adsorbed on Au(111), according to the lowest-energy transition path $Au(ads)_a$ in Figure 4. For the reaction **2** → **2′**, the anthracene units have been labeled **A**−**D**, where **A** and **D** are the units terminating the molecules, while **B** and **C** denote the central segments.

First, consider the triggering of reaction **2** → **2′**: 1.10 eV is required to obtain the first covalent coupling between the two central units **B** and **C**, while it costs only 0.31 eV to get the first link between units **A** and **B** at one end of the molecule. Furthermore, the second coupling is also easier to realize between the partially coupled units **A** and **B** than between the central units **B** and **C** (compare 0.39 to 0.89 eV). Once the two links between **A** and **B** have been established, the energy cost for linking **B** and **C** is reduced to 0.08 and 0.18 eV for the first and second connections, respectively.

In the reaction from an extended polyanthracene into a GNR, most anthracene units will be similar to units **B** and **C**. Therefore, the reaction energies of the steps **2b′** → **2c′** and **2c′** → **2d** are the most important data presented in Figure 5, as they correspond to the two dehydrogenation energies in the middle of a large molecule and provide a good indication for most of the polymerization energies required. We note that the reaction **2b′** → **2c″** is less representative for a long GNR, as it is actually very similar to the initiation of the cyclodehydrogenation from the other end of the molecule.

The results in Figure 5 show that the energy cost of a random cyclodehydrogenation anywhere along the polyanthracene is around 1.10 eV (reaction **2** → **2a**″). However, the cost of creating the first new C−C coupling adjacent to an existing one is drastically reduced to 0.08 eV (reaction **2b**′ → **2c**′). This suggests that the cyclodehydrogenation reaction is initiated at one end of the polyanthracene and then propagates unit-by-unit through the entire polymer in a domino-like fashion. The cyclodehydrogenation reaction therefore corresponds to *positive cooperativity*[24] by which the probability of any given coupling is drastically increased if a neighboring coupling already exists.

By considering the overall reaction energies, we find that **1** → **1**′ is slightly exothermic, with an energy gain of about 50 meV per C−C bond formed. **2** → **2**′, on the other hand, is endothermic, with an energy loss around 70 meV per C−C coupling. Extrapolating this trend for the cyclodehydrogenation of polyanthracene to our GNR, one may expect the reaction energy to increase further to become even more endothermic than **2** → **2**′. These net reaction energies are a result of a delicate balance between an energy gain through the closer adsorption of the product and a net energy loss resulting from the dehydrogenation and the formation of a C−C bond.

In conclusion, we have established how the on-surface synthesis of a graphene nanoribbon proceeds on the Au(111) surface. From transition-state calculations, it was found that the Au(111) surface catalyzes the cyclodehydrogenation: H-atoms are pulled onto the surface in a concerted first step, followed by a separate desorption into the vacuum. This reaction has only one energy barrier, while the other conceivable reaction paths have an intermediate minimum followed by a high energetic barrier. For the complete cyclodehydrogenation, the net energy gain of a four-anthracene molecule was found to be smaller than the reaction energy for the dianthracene precursor. From this information, one can extrapolate that the overall reaction for a long GNR is slightly less favorable and it could even be energy neutral. This is an effect of the variation in hydrogen-to-carbon ratios of different PAHs, and we conclude that the binding energy of a PAH depends linearly on this ratio. Finally, we show that the cyclodehydrogenation of polyanthracene is most likely to start at one end of the polymer and propagates with a domino-like effect throughout the polymer. This conclusion is also expected to be relevant for other polyphenyl-based GNR precursors where steric hindrance plays an important role for the cyclodehydrogenation.

■ ASSOCIATED CONTENT

Supporting Information. Computational details, additional figures, and data tables. This material is available free of charge via the Internet at http://pubs.acs.org.

■ AUTHOR INFORMATION

Corresponding Author
sven.stafstrom@liu.se; hanke@liverpool.ac.uk

■ ACKNOWLEDGMENT

A. Gulans, Prof. M. Puska, and Prof. R. Nieminen at Aalto University are acknowledged for their implementation of the vdW-DF, and Dr. C.-A. Palma at MPI for Polymer Research for his inspiration. Funding was provided by the Swedish Research Council and computer recourses were allocated by the National Supercomputer Centre, Sweden through SNAC and the MATTER consortium.

■ REFERENCES

(1) Novoselov, K. S.; Geim, A.; Morozov, S. V.; Jiang, D.; Zhang, Y.; Dubonos, S. V.; Grigorieva, I. V.; Firsov, A. A. *Science* **2004**, *306*, 666–669.
(2) (a) Nakada, K.; Fujita, M.; Dresselhaus, G.; Dresselhaus, M. S. *Phys. Rev. B* **1996**, *54*, 17954–17961. (b) Barone, V.; Hod, O.; Scuseria, G. E. *Nano Lett.* **2006**, *6*, 2748–2754. (c) Yang, L.; Park, C.-H.; Son, Y.-W.; Cohen, M. L.; Louie, S. G. *Phys. Rev. Lett.* **2007**, *99*, 186801–1868004.
(3) Chen, Z.; Lin, Y.-M.; Rooks, M. J.; Avouris, P. *Physica E* **2007**, *40*, 228–232.
(4) Tapasztó, L.; Dobrik, G.; Lambin, P.; Biró, L. P. *Nature Nanotechnol.* **2008**, *3*, 397–401.
(5) Sprinkle, M.; Ruan, M.; Hu, Y.; Hankinson, J.; Rubio-Roy, M.; Zhang, B.; Wu, X.; Berger, C.; de Heer, W. A. *Nature Nanotechnol.* **2010**, *5*, 721–731.
(6) (a) Kosynkin, D. V.; Higginbotham, A. L.; Sinitskii, A.; Lomeda, J. R.; Dimiev, A.; Price, B. K.; Tour, J. M. *Nature* **2009**, *458*, 872–876. (b) Jiao, L.; Wang, X.; Diankov, G.; Wang, H.; Dai, H. *Nature Nanotechnol.* **2010**, *5*, 321–325.
(7) Cai, J.; Ruffieux, P.; Jaafar, R.; Bieri, M.; Braun, T.; Blankenburg, S.; Muoth, M.; Seitsonen, A. P.; Saleh, M.; Feng, X.; Müllen, K.; Fasel, R. *Nature* **2010**, *466*, 470–473.
(8) Grill, L.; Dyer, M.; Lafferentz, L.; Persson, M.; Peters, M. V.; Hecht, S. *Nature Nanotechnol.* **2007**, *2*, 687.
(9) Haq, S.; Hanke, F.; Dyer, M. S.; Persson, M.; Iavicoli, P.; Amabilino, D. B.; Raval, R. *J. Am. Chem. Soc.* **2011**, *133*, 12031.
(10) (a) Palma, C.-A.; Samorì, P. *Nature Chem.* **2011**, *3*, 431–436. (b) In't Veld, M.; Iavicoli, P.; Haq, S.; Amabilino, D. B.; Raval, R. *Chem. Commun.* **2008**, 1536–1538. (c) Matena, M.; Riehm, T.; Stöhr, M.; Jung, T. A.; Gade, L. H. *Angew. Chem., Int. Ed.* **2008**, *47*, 2414–2417. (d) Matena, M.; Stöhr, M.; Riehm, T.; Björk, J.; Martens, S.; Dyer, M. S.; Persson, M.; Lobo-Checa, J.; Müller, K.; Enache, M.; Wadepohl, H.; Zegenhagen, J.; Jung, T. A.; Gade, L. H. *Chem.—Eur. J.* **2010**, *16*, 2079–2091.
(11) Treier, M.; Pignedoli, C. A.; Laino, T.; Rieger, R.; Müllen, K.; Passerone, D.; Fasel, R. *Nature Chem.* **2011**, *3*, 61–67.
(12) (a) Bieri, M.; Nguyen, M.-T.; Gröning, O.; Cai, J.; Treier, M.; Aït-Mansour, K.; Ruffieux, P.; Pignedoli, C. A.; Passerone, D.; Kastler, M.; Müllen, K.; Fasel, R. *J. Am. Chem. Soc.* **2010**, *132*, 16669–16676. (b) Blankenburg, S.; Rauls, E.; Schmidt, W. G. *J. Phys. Chem. Lett.* **2010**, *1*, 3266–3270. (c) Nguyen, M.-T.; Pignedoli, C. A.; Passerone, D. *Phys. Chem. Chem. Phys.* **2011**, *13*, 154–160.
(13) (a) Kresse, G.; Furthmüller, J. *Phys. Rev. B* **1996**, *54*, 11169–11186. (b) Blöchl, P. E. *Phys. Rev. B* **1994**, *50*, 17953–17979. (c) Kresse, G.; Joubert, D. *Phys. Rev. B* **1999**, *59*, 1758–1775.
(14) Bahn, S.; Jacobsen, K. *Comp. Sci. Eng.* **2002**, *4*, 56–66.
(15) (a) Dion, M.; Rydberg, H.; Schröder, E.; Langreth, D. C.; Lundqvist, B. I. *Phys. Rev. Lett.* **2004**, *92*, 246401–246404. (b) Gulans, A.; Puska, M. J.; Nieminen, R. M. *Phys. Rev. B* **2009**, *79*, 201105–201108.
(16) Mura, M.; Gulans, A.; Thonhauser, T.; Kantorovich, L. *Phys. Chem. Chem. Phys.* **2010**, *12*, 4759–4767.
(17) Perdew, J. P.; Burke, K.; Ernzerhof, M. *Phys. Rev. Lett.* **1996**, *77*, 3865–3868.
(18) Björk, J.; Hanke, F.; Palma, C.-A.; Samorì, P.; Cecchini, M.; Persson, M. *J. Phys. Chem. Lett.* **2010**, *1*, 3407–3412.
(19) (a) Jónsson, H.; Mills, K. W. J. In *Classical and Quantum Dynamics in Condensed Phase Simulations*; Berne, B. J., Ciccotti, G., Coker, D. F., Eds.; World Scientific: Singapore, 1998; pp 385−404. (b) Henkelman, G.; Uberuaga, B.; Jónsson, H. *J. Chem. Phys.* **2000**, *113*, 9904. (c) Henkelman, G.; Jónsson, H. *J. Chem. Phys.* **2000**, *113*, 9978–9985.
(20) (a) Henkelman, G.; Jónsson, H. *J. Chem. Phys.* **1999**, *111*, 7010–7022. (b) Kästner, J.; Sherwood, P. *J. Chem. Phys.* **2008**, *128*, 014106–014111.
(21) Wornat, M. J.; Sarofim, A. F.; Lafleur, A. L. The Pyrolysis of Anthracene as a Model Coal-Derived Aromatic Compound. *Proceedings of the 24th International Symposium on Combustion*; The Combustion Institute: Pittsburgh, PA, 1992; p 955.
(22) Hänggi, P.; Talkner, P.; Borkovec, M. *Rev. Mod. Phys.* **1990**, *62*, 251–341.
(23) Hammer, B.; Nørskov, J. K. *Nature* **1995**, *376*, 238–240.
(24) Hunter, C. A.; Anderson, H. L. *Angew. Chem., Int. Ed.* **2009**, *48*, 7488–7499.